Parametric Effects of Heat and Mass Transport on Steady Hydrodynamics Viscoelastic Fluid Flow with Soret-Dufour in Porous Materials

MFEBE, J. F[1], AMOO, S. A[2], ANYANWU, E. O[3]
[1,2,3]Department of Mathematics, Federal University Wukari, Nigeria

Abstract- The study aimed to present graphically the analysis of various parameters that explain soret-dufour effects on heat and mass transport of hydrodynamics viscoelastic flow in porous materials, with primary objectives of developing a mathematical model that describes the system. We derived a nonlinear mathematical model for the parametric effects of fluids on energy generation and efficiency, and solve the nonlinear model numerically to determine the effects of dimensionless parameters on heat and mass transport in porous materials with soret-dufour effects. The emanating partial differential equations were reduced to couple nonlinear ordinary differential equations with transformation similarities. Embedded fourth order Runge-Kutta method with shooting techniques were used to simplify the ordinary differential equations which represent convective heat and mass transport. The results showed significant changed in Dufour and Soret, where decreased in Nusselt was noticed in Dufour but increased in Soret. Also increased in velocity profile but decreased in Sherwood and Nusselt number respectively. Increased in radiation parameter led to corresponding increased in velocity profile and Sherwood numbers but not in Nusselt number. Concluding that solutal Grashof number, thermal Grashof number, magnetic parameter, radiation parameter, Dufour and Soret effects had significant effects on hydrodynamic viscoelastic fluid flow in porous materials.

Indexed Terms- Parameric, Hydrodynamics, Viscoelastic, Dufour, Soret

I. INTRODUCTION

The world at large is undergoing energy insufficiency, due to the growing population and industrialization processes taking place in the globe. Hence the need to device other sources of energies, other than the fossil fuel resource, as such it is very important to study new energies sources and how it can be put to global use, enhancing productivity and reducing cost. In this findings, our efforts are to reflect the effects of dimensionless parameter on steady hydrodynamics viscoelastic parameters in explaining viscoelasticity in porous materials, as it has wide and numerous applications in industries and environments (Kala, Singh and Kumar, 2014, Amoo, 2022). Some areas of applications of this findings are the flow of ground water through soil and

rocks which are of great important in agriculture and pollution control, extraction of oil and natural gas from rocks as are prominent in oil and gas industries, functioning of tissues in body belong to porous surfaces, flow of blood and treatments through them, understanding various medical conditions (tumor growth, formation of porous material) and their treatment (injection, flow in medical sciences) though not limited to those mentioned. The interaction of magnetic fields with viscoelastic fluids is of particular interest, as these fluids exhibit memory effects and elasticity in addition to viscosity, which significantly alters the flow behavior compared to Newtonian fluids (Sadeghy et al. 2001; Hayat et al., 2008, Amoo and Idowu, 2018). A material property that exhibits both viscous and elastic characteristics and undergoing deformation when external force is applied is viscoelastic (Gizachew and Shankar, 2018). Hydrodynamics viscoelastic flow fluid widescreen with respect to the radiation source/heat sink (non-uniform) of the energy equation has been studied by Nandeppanavar et al. 2011, Gizachew and Shankar, 2018). They noted that the PHF boundary conditions are more suitable for the effective cooling spreadsheet. Many researchers have investigated hydrodynamic viscoelastic fluid flow on heat transfer in over a stretching sheet with viscous dissipation, internal heat generation/absorption, and radiation (Sidheswar and Mahabalewar 2005, Gizachew and Shankar, 2018, Amoo and Idowu, 2018, Mfebe Amoo and Anyanwu, 2025). They came to similar conclusion, that the later affects the transport system. Heydari and Taleghani, (2016), studied fluid flow and heat transfer in non-Newtonian viscoelastic fluid and hydrodynamic steady laminar flow expanded on a horizontal plane. Several studies have focused individually on aspects such as MHD flow, viscoelastic effects, cross-diffusion phenomena, and porous media flow. However, limited attention has been paid to the combined influence of soret-dufour effects on hydrodynamic viscoelastic on steady boundary layer behavior in porous materials. The present study aims to fill this research gap This analysis is vital for enhancing the understanding of complex fluid flow mechanisms and for improving the efficiency of industrial and engineering processes involving such flows.

II. MATHEMATICAL FORMULATION

Hydrodynamic viscoelastic thermal effects on heat and mass transport is considered of an electrically conducting steady compressible fluid past a stretched sheet under the action of thermal and solutal buoyancy forces, with uniformly transverse variable magnetic field B(x) applied at right angle to the direction of flow with chemical reaction taking place in the flow. The transverse applied magnetic field and induced magnetic, are assumed to be very small, so that the induced magnetic field is negligible. The flow is assumed to be in the x-direction with y-axis normal to it with velocity $Uw(x)$, temperature distribution $Tw(x)$, $\gamma 0$, the newtonian viscoelastic parameter, g is the acceleration due to gravity, $\boldsymbol{\lambda}$ is the chemical reaction parameter and concentration distribution $Cw(x)$ moving through a quiescent ambient fluid of constant temperature $T1$ and concentration $C1$. The presence of thermal diffusion (Soret) and diffusion-thermo (Dufour) effects were included. The plate is maintained at the temperature and species concentration Tw, Cw and free stream temperature and species concentration$T1$, $C1$ respectively. The equations governing the flow effects of heat and mass transfer of steady hydrodynamic viscoelastic fluid flow in porous materials are detailed. In this study we considered a steady 2-D compressible fluid which is a Newtonian flow in stretching sheet.

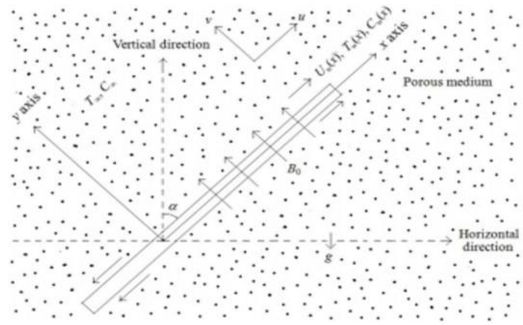

Figure 1: The Geometry of the Model and Coordinate System (Bidyut et al, 2020).

Continuity equation

$$\frac{\partial u}{\partial x} + \frac{\partial v}{\partial y} = 0 \qquad (1)$$

Momentum equation

$$u\frac{\partial u}{\partial x} + v\frac{\partial u}{\partial y} = -\left(\frac{1}{\rho}\sigma B^2(x) + \frac{\nu}{K}\right)u + \nu\frac{\partial^2 u}{\partial y^2} - \gamma_0\left\{u\frac{\partial^3 u}{\partial x\,\partial y^2} + v\frac{\partial^3 u}{\partial y^3} + \frac{\partial u}{\partial x}\frac{\partial^2 u}{\partial y^2}\right\} + g\beta_T(T - T_\infty) + g\beta_C(C - C_\infty)$$

(2)

Energy equation

$$\rho C_p\left(u\frac{\partial T}{\partial x} + v\frac{\partial T}{\partial y}\right) = k\frac{\partial^2 T}{\partial y^2} - \frac{\partial q_r}{\partial y} + Q_0(T - T_\infty) + \frac{D_m \partial^2 C}{C_s \partial y^2}$$

(3)

concentration equation

$$u\frac{\partial C}{\partial x} + v\frac{\partial C}{\partial y} = D\frac{\partial^2 C}{\partial y^2} - \gamma(C - C_\infty) + \frac{D_m \partial^2 T}{T_m \partial y^2} \qquad (4)$$

The boundary condition governing the flow are;

$$u = U_0 e^{\frac{x}{l}}, v = -V e^{\frac{x}{l}}, T = T_w + T_0 e^{\frac{x}{2l}}, C = C_w + C_0 e^{\frac{x}{2l}}, at\ y = 0$$

$$u \rightarrow 0, T \rightarrow T_\infty, C \rightarrow C_\infty,\ y \rightarrow \infty, y \rightarrow \infty \tag{5}$$

By using Rossland approximation according to (Ibrahim and Suneetha, 2015, Amoo and Idowu, 2018) we have;

$$q_r = -\frac{4\sigma 0}{3\delta}\frac{\partial T^4}{\partial y} \tag{6}$$

Considering temperature differences in the flow are small such that $T4$ may be expressed as a linear function of temperature and using Taylor series expand of $T4$ about the neighborhood $T\infty$ and neglecting higher order terms, this gives the approximation.

$$T^4 \cong 4T_\infty^3 T - 3T_\infty^4 \tag{7}$$

Follow from (6) and (7), that equation (4) becomes

$$\left(u\frac{\partial T}{\partial x} + v\frac{\partial T}{\partial y}\right) = \left(\frac{k}{\rho C_p} + \frac{16\sigma 0 T_\infty^3}{3\delta\rho C_p}\right)\frac{\partial^2 T}{\partial y^2} + \frac{Q0}{\rho C_p}(T - T\infty) + \frac{Dm\partial^2 C}{\rho C p C_s \partial y^2} \tag{8}$$

$B(x)$, the magnetic field is considered to be in the form

$$B(x) = \mathrm{B}_0^2 e^{\frac{x}{2l}} \tag{9}$$

Where $B0$ is a constant magnetic field.

We now introduce the stream function $\boldsymbol{\psi}$(x,y) such that

$$u = \frac{\partial \psi}{\partial y} \qquad , v = -\frac{\partial \psi}{\partial x} \tag{10}$$

We substitute (10) into (1), we have the Cauchy Riemann equation, which states that given a function $F(z) = u(a, b) + iv(a, b)$, and z = a + ib, and u(a, b) and v(a, b) are real-valued functions. Then, $F(z) = u(a, b) + iv(a, b)$ is analytic at $z0$ if and only if the following Cauchy- Riemann equations hold:

$$\frac{\partial u}{\partial x} = \frac{\partial v}{\partial y} \qquad and \quad \frac{\partial u}{\partial y} = -\frac{\partial v}{\partial x} \tag{11}$$

hence the continuity condition (1) is fully satisfied.

$$\frac{\sigma}{\partial x}\left(\frac{\sigma\psi}{\partial y}\right) - \left(\frac{\sigma}{\partial y}\right)\left(\frac{\sigma\psi}{\partial x}\right) = 0 \tag{12}$$

Considering (10) in equations (2, 3 and 4) they become;

$$\frac{\partial\psi}{\partial y}\frac{\partial^2\psi}{\partial x\partial y} - \frac{\partial\psi}{\partial x}\frac{\partial^2\psi}{\partial y^2} = \mathrm{v}\frac{\partial^3\psi}{\partial y^3} - \left(\frac{1}{\rho}\sigma B_0^2 e^{\frac{x}{2L}} + \frac{\mathrm{v}}{\mathrm{K}}\right)\frac{\partial\psi}{\partial y} - \Upsilon_0\left\{\frac{\partial\psi}{\partial y}\frac{\partial^3 u}{\partial x\partial y^2} + \mathrm{v}\frac{\partial^3\psi}{\partial y^3} + \frac{\partial u}{\partial x}\frac{\partial^2 u}{\partial y^2}\right\} + g\beta_r(T - T_\infty) + g\beta_C(C - C_\infty) \tag{13}$$

$$\left(\frac{\partial\psi}{\partial y}\frac{\partial T}{\partial x} - \frac{\partial\psi}{\partial x}\frac{\partial T}{\partial y}\right) = \left(\frac{k}{\rho C_p} + \frac{16\sigma 0 T_\infty^3}{3\delta\rho C_p}\right)\frac{\partial^2 T}{\partial y^2} + \frac{Q0}{\rho C_p}(T - T\infty) + \frac{Dm\partial^2 C}{C_s\partial y^2} \tag{14}$$

$$\frac{\partial\psi}{\partial y}\frac{\partial C}{\partial x} - \frac{\partial\psi}{\partial x}\frac{\partial C}{\partial y} = D\frac{\partial^2 C}{\partial y^2} - \gamma(C - C_\infty) + \frac{Dm\partial^2 T}{Tm\partial y^2} \tag{15}$$

The corresponding boundary conditions become:

$$\frac{\partial\psi}{\partial y} = U_0 e^{\frac{x}{l}}, \frac{\partial\psi}{\partial x} = V_0 e^{\frac{x}{l}}, T = T_w = T_\infty + T_0 e^{\frac{x}{2l}}, C = C_w = C_\infty + C_0 e^{\frac{x}{2l}}, at\ y = 0,$$

$$\frac{\partial\psi}{dy} \rightarrow 0, T \rightarrow T_\infty, C \rightarrow C_\infty, as\ y \rightarrow \infty \tag{16}$$

In order to transform the equation (13), (14) and (15) into ordinary differential equations, we apply similarity variable (17) according (Sajid and Hayat, 2008; Amoo and Idowu, 2018).

$$\psi(x, y) = \sqrt{2vU_0 l}\, e^{\frac{x}{2l}} f(\eta), \eta = y\sqrt{\frac{U_0}{2vl}}\, e^{\frac{x}{2l}}, T = T_\infty + T_0 e^{\frac{x}{2l}}\theta(\eta), C = C_\infty + C_0 e^{\frac{x}{2l}}\phi(\eta)$$

(17)

Since the continuity equation has been fully satisfied, we define the following dimensionless parameters

$$M = \frac{2\sigma l B_0^2}{\rho U_0} e^{\frac{x}{2l}}, Pr = \frac{\mu v C_p}{K}, R = \frac{4\sigma_0 T_\infty^3}{\delta K}, Sc = \frac{v}{Dm}, f_w = V_0\sqrt{\frac{2l}{vU_0}}\, e^{-\left(\frac{x}{2l}\right)}, \lambda = \frac{2vl}{U_0} e^{-\left(\frac{x}{l}\right)}$$

$$Q = \frac{2lQ_0}{U_0\rho Cp} e^{-\left(\frac{x}{l}\right)}, D_u = \frac{D_m U_0}{C_s 2vl} C_0 e^{\frac{3x}{2l}}, S_r = \frac{D_m U_0}{T_m 2vl} T_0 e^{\frac{3x}{2l}}, D_a = \frac{2vl}{U_0 K} e^{-\left(\frac{x}{l}\right)}$$

$$G_r = \frac{2lg\beta_T T_0}{U_0^2} e^{\frac{3x}{2l}}, G_C = \frac{2lg\beta_C C_0}{U_0^2} e^{\frac{3x}{2l}} \tag{18}$$

Method of the solution

By following similar steps as that of Amoo and Idowu, (2018), A Shooting technique alongside embeded fouth order Runge-Kutta method has been adopted as the numerical scheme for this research work. It is a step by step process where a table of function values for a range of values of x is accumulated. Several intermediate calculations are required at each stage, but these are straight forward and present little difficulty. Shooting method reformulates the BVP to Initial Value Problem (IVP) by adding sufficient number of conditions at one end and adjust these conditions until the given conditions are satisfied at the other end while Runge Kutta method solve the initial value problems. Summary to the steps are: (i) the method replaced the given BVP to sequence IVPs, (ii) Integrating the sequence of IVPs using embedded fourth order Runge-Kutta scheme, (iii) The integration length varies with the parameter values and it has been suitably chosen each time such that the boundary conditions at the outer edge of boundary layer are satisfied, and (iv) Repeating this procedure till the convergence is obtained satisfying the boundary conditions. The governing equations of the system are essentially nonlinear ordinary differential equations together with the boundary conditions are solved numerically. The method has been proven to be adequate for boundary layer equations, seems to give accurate results and has been widely used (Ibrahim and Makinde, 2010, Ibrahim and Suneetha, 2015, Amoo and Idowu, 2017, 2018).

$$y_{n+1} = y_n + \frac{\Delta\eta}{6}(N_1 + 2N_2 + 2k_3 + N_4) \quad (19)$$

Where

$$N_1 = \Delta\eta f(x_n, y_n)$$

$$N_2 = \Delta\eta f\left(x_n + \frac{\Delta\eta}{2}, y_n + \frac{k_1}{2}\right)$$

$$N_3 = \Delta\eta f\left(x_n + \frac{\Delta\eta}{2}, y_n + \frac{k_2}{2}\right)$$

$$N_4 = \Delta\eta f(x_n + \Delta\eta, y_n + k_3)$$

Where $\Delta\eta$=0.01 is the step size. Hence the following ordinary differential equations are obtained from the transform similarity variable

$$f''' + ff'' - 2(f')^2 - (M + Da)f' - \lambda_1[2f'f''' - ff^4 - f''^2] + G_T\theta + G_c\Phi \quad (20)$$

$$\left(1 + \frac{4}{3}R\right)\theta'' + Prf\theta' - Prf'\theta - PrQ\theta + P_rD_f\phi'' = 0 \quad (21)$$

$$\Phi'' + S_cf\Phi' - Scf'\phi - S_c\lambda\theta + S_cS_r\theta'' = 0 \quad (22)$$

with corresponding transformed boundary conditions takes the form;

$f = fw$, $f' = 1$, $\theta = 1$, $\Phi = 1$, $at\ \eta = 0$

$f' = 0$, $\theta = 0$, $\phi = 0$, $as\ \eta \to \infty$ (23)

Equations (20, 21, and 22) were integrated as IVPs with embedded fourth order Runge-Kutta method for $f''(0)$, $\theta'(0)$ and $\phi'(0)$ which are require to explain velocity, Nusselt and Sherwood numbers, were not given at the boundary. The suitable guess values for $f''(0)$, $\theta'(0)$ and $\phi'(0)$ were chosen and then integration was carried out. Calculated values for $f''(0)$, $\theta'(0)$ and $\phi'(0)$ at η = 7 with the given boundary conditions $f''(7) = 0$, $\theta'(7) = 0$ and $\phi'(7) = 0$, were compared obtained values which were then adjusted to estimate values for $f''(0)$, $\theta'(0)$ and $\phi'(0)$, to give a better approximation for the solution. By performing series of computations to obtain values for $f''(0)$, $\theta'(0)$ and $\phi'(0)$, with step-size $\Delta\eta$ = 0.01. The above procedure was repeated to obtained results up to the desired degree of accuracy 10−6 These enabled us to use the effects of dimensionless parameters to explain soret-dufour effects on heat and mass transport of steady hydrodynamic viscoelastic fluid flow. However, the physical quantity of practical interest are the velocity profile, the Nusselt and Sherwood number defined respectively as:

$$C_f = \frac{T_w}{\rho u_w^2}, Nu = \frac{q_w x}{k(T_w - T_\infty)}, Sh = \frac{q_m x}{D_m(C_w - C_\infty)} \quad (24)$$

Where k is the thermal conductivity of the fluid, Tw, qw, and qm are respectively given as;

$$T_w = \mu\left(\frac{\partial u}{\partial y}\right)_{y=0}, q_w = k\left(\frac{\partial T}{\partial y}\right)_{y=0}, q_m = D\left(\frac{\partial T}{\partial y}\right)_{y=0} \quad (25)$$

Therefore, the velocity profile, Nusselt and Sherwood number are:

$$C_f Re_x^{\frac{1}{2}} = f''(0), \; Nu Re_x^{\frac{1}{2}} = \theta'(0), \; Sh Re_x^{-(\frac{1}{2})} = \Phi'(0) \qquad (26)$$

$Re^{\frac{1}{2}} = \frac{U_w x}{v}$ is the local Reynolds number.

Therefore, Cf, Nu, and Sh are rewritten respectively as:

$$C_f \left(\frac{U_w x}{v}\right)^{-\frac{1}{2}} = f''(0), \; Nu\left(\frac{U_w x}{v}\right) = \theta'(0), \; Sh\left(\frac{U_w x}{v}\right)^{\frac{1}{2}} = \Phi'(0) \qquad (27)$$

III. RESULT AND DISCUSSION

The variation of parameters and numerical computation of the results are revealed, the effect of dimensionless parameters on hydrodynamic viscoelastic flow in porous materials are revealed. Our focus been the effects on velocity profile, Nusselt and Sherwood numbers, which are respectively $f''(0)$, $\theta'(0)$ and $\phi'(0)$. Solving the nonlinear model numerically, using maple 2024 embedded classical fourth order Runge-Kutta scheme alongside a shooting technique. Table 1.1, shows the comparison of the present study with previous studies, using the same values as the existing works from the literature review for $\theta'(0)$ and $\phi'(0)$ by maintaining all newly introduced parameters zero, so as to be able to compare steady hydrodynamic viscoelastic fluid flows. The numerical values of $\theta'(0)$ and $\phi'(0)$ at the sheet for different values of Gr, Gc, M, fw, Pr and Sc was done to validate our result. From the table it could be deduced that the variations of Gr. =Gc. = M = fw= 0.1 for numerical values of θ'(0) and φ'(0) at the sheet when compared with the existing literature were in close agreement. A comparison of the previous studies over years had been improvement for Gr = Gc= M= fw =0.1 and the present study followed the same trends of improved results. The possible reasons for the trends in variation might be due to accuracy of the method of solution and system of equations or models considered.

Table 1.1 comparing present study with previous study for $\theta'(0)$ and φ'(0) for Steady hydrodynamic viscoelastic fluid flow for different values of Gr, Gc, M, Fw, Sc Pr.

Present study (2025)								Amoo & Idowu, (2018)		Lakshmi *et al.* (2012)	
Gr	Gc	M	Fw	Sc	Pr	- φ'(0)	$-\theta'(0)$	- φ'(0)	$-\theta'(0)$	- φ'(0)	$-\theta'(0)$
0.1	0.1	0.1	0.1	0.62	0.5	0.752641	0.651008	0.74019	0.80508	0.728481	0.79904
0.5	0.1	0.1	0.1	0.62	0.5	0.720677	0.621562	0.77380	0.84101	0.76248	0.83593
1.0	0.1	0.1	0.1	0.62	0.5	0.687004	0.591016	0.806773	0.87617	0.79681	0.87297
0.1	0.5	0.1	0.1	0.62	0.5	0.798879	0.694902	0.776285	0.843609	0.76491	0.83850
0.1	0.1	0.1	0.1	0.78	0.5	0.875235	0.648650	0.84118	0.803798	0.83297	0.79369

M = 1, Gr = 1, Gc = 0.01, fw = 1, Q = 0.5, R = 0.5, Sc = 0.35, P r = 0.31, Du =0.02, Sr =0.035, λ = 0. All the computations on table 1.2 were carried out using the values these parameters except otherwise indicated on the graph.

Table 4.2: Effects of Dimensionless parameters on f ''(0), θ'(0) and ϕ'(0)

P	Values	$-f''(0)$	$-\theta'(0)$	$-\phi'(0)$	P	Values	$-f''(0)$	$-\theta'(0)$	$\phi'(0)$
M	1	1.589606	0.577131	0.725277	Da	0.001	0. 1.485577	461475	0.457614
	3	2.236783	0.545029	0.660935		1	1.485577	0.461475	0.457614
	5	2.780869	0.932972	0.595001		2.5	2.161419	0.378830	0.421999
	7	3.132035	0.514279	0.594703		3.5	2.380086	0.359401	0.413778
Gc	0.01	1.485577	0.461475	0.457614	Gr	1	1.589606	0.577131	0.725277
	3.10	1.095649	0.538770	0.493634		2	1.086034	0.609669	0.785255
	3.80	1.014232	0.550814	0.499729		3	0.626590	0.634838	0.828979
	4.50	0.934508	0.561819	0.505396		4	0.196133	0.655735	0.864010
Fw	1	1.485577	0.577134	0.725271	Pr	0.24	1.559031	0.494189	0.736283
	2	2.185879	0.680571	0.966075		0.31	1.589605	0.577137	0.725282
	3	2.935640	0.801246	1.241991		0.62	1.689349	0.903510	0.689385
	4	3.802415	0.937828	1.541983		1.24	1.804010	1.465574	0.650663
R	0.5	1.485577	0.461475	0.457614	Q	0.5	1.485577	0.461475	0.457614
	2	1.463977	0.481260	0.206521		1.5	1.499800	0.448756	0.642531
	5	1.473039	0.472949	0.306133		2.5	1.508733	0.441166	0.781495
	7	1.465890	0.479510	0.226980		3.5	1.515217	0.435905	0.897427
Sc	0.35	1.485577	0.461475	0.457614	Du	0.02	1.485577	0.461475	0.457614
	0.62	1.485709	0.726337	0.456732		0.2	1.484951	0.462045	0.449011
	1.50	1.485863	1.138686	0.455324		2	1.478599	0.467733	0.361642
	2.00	1.486007	1.738185	0.453218		4	1.471349	0.474012	0.261733
Sr	0.035	1.485577	0.461475	0.457614	λ	1	1.590197	0.578938	0.727308
	0.5	1.485550	0.484904	0.4577767		1.25	1.723961	0.603423	0.788957
	1.50	1.485492	0.314614	0.458095		1.50	1.867224	0.626712	0.840521
	2	1.485463	0.264969	0.458260		1.75	2.021504	0.653099	0.902111

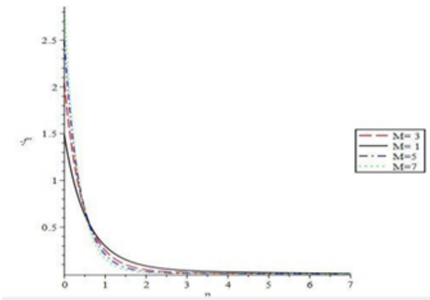

Fig 1 Hartmann number, M on f’’

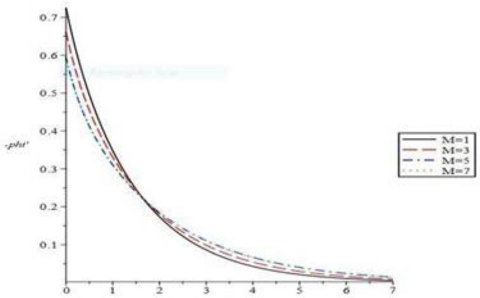

Fig 2 Hartmann number, M on ϕ’

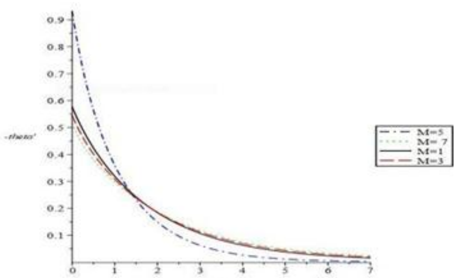

Fig 3 Hartmann number, M on θ’

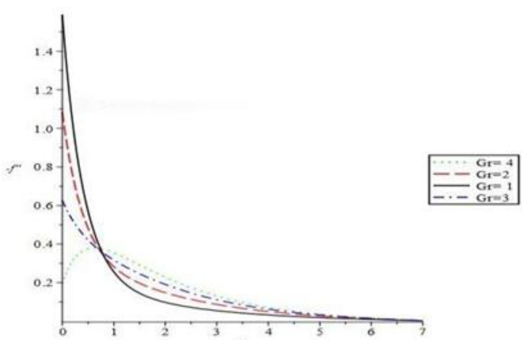

Fig 4 Grashof number, Gr on f’’

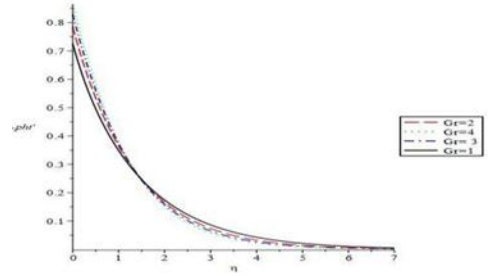

Fig 5 Grashof number, Gr on ϕ’

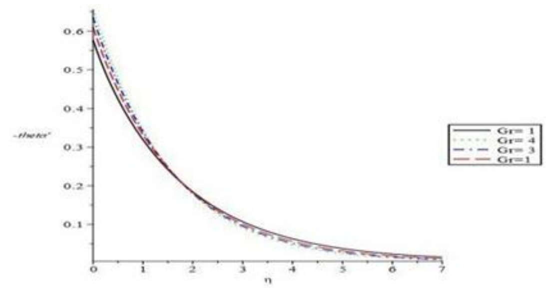

Fig 6 Grashof number, Gr on θ’

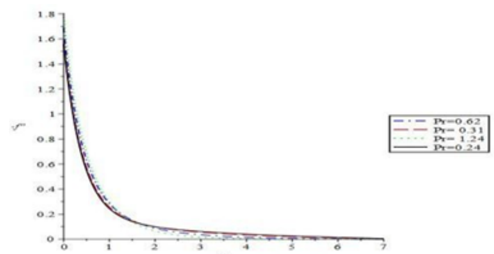

Fig 7 Prandlt number, Pr on f’’

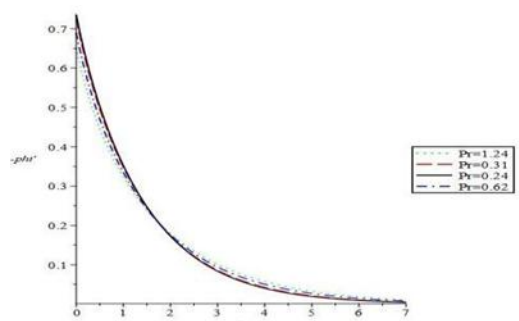

Fig 8 Prandlt number, Pr on ϕ’

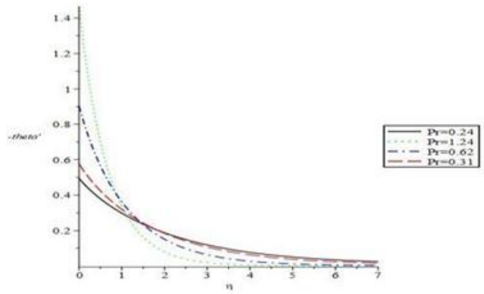

Fig 9 Prandlt number, Pr on θ’

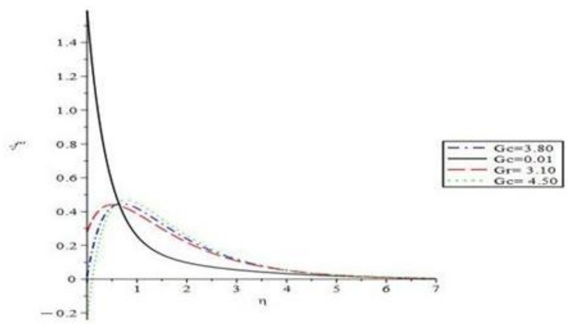

Fig10 Solutal Grashof number, Gc on f’’

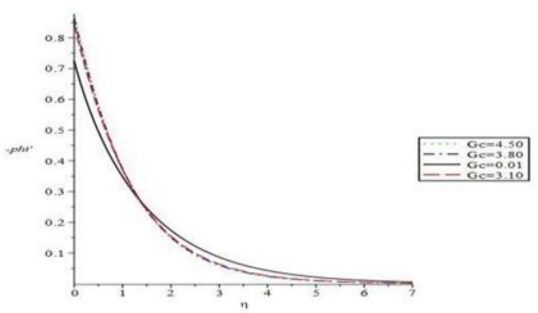

Fig 11 Solutal Grashof number, Gc on ϕ’

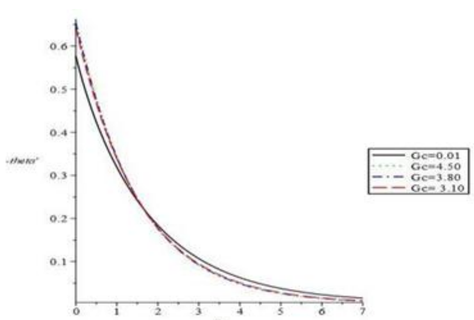

Fig 12 Solutal Grashof number, Gc on θ

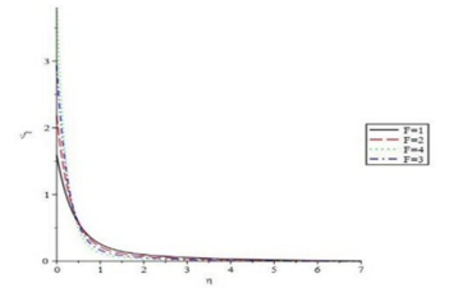

Fig 13 skin friction, Fw on f’’

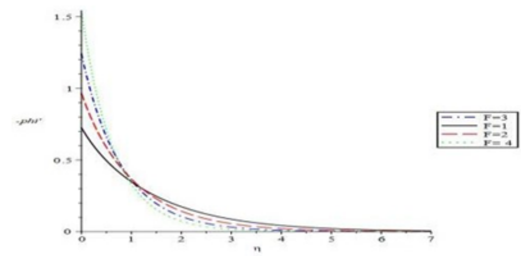

Fig 14 Skin friction, Fw on ϕ’

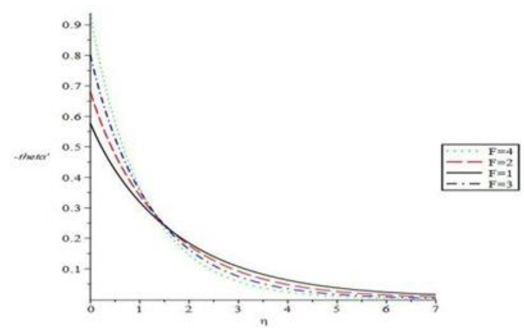

Fig 15 Skin friction, Fw on θ

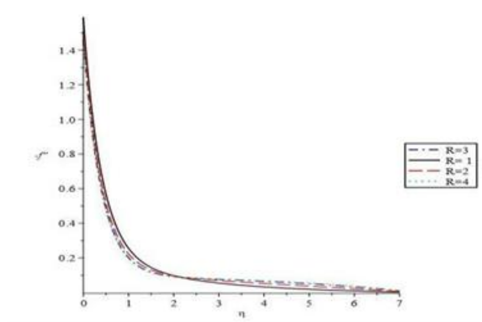

Fig 16 thermal radiation, R on f’’

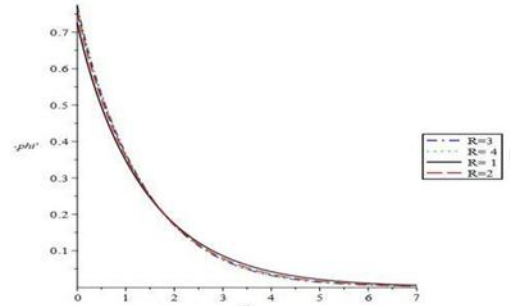

Fig 17 thermal radiation, R on ϕ’

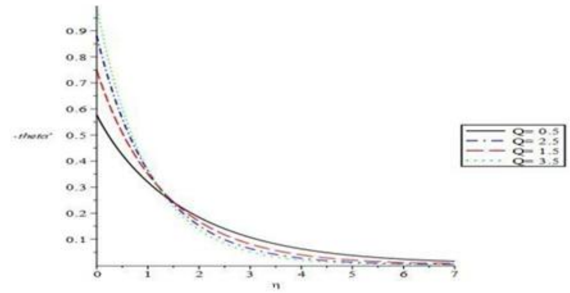

Fig 21 thermal heat generation, Q on θ

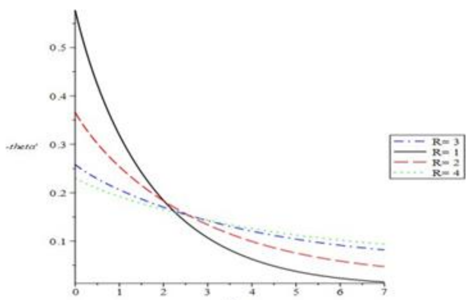

Fig 18 thermal radiation, R on θ

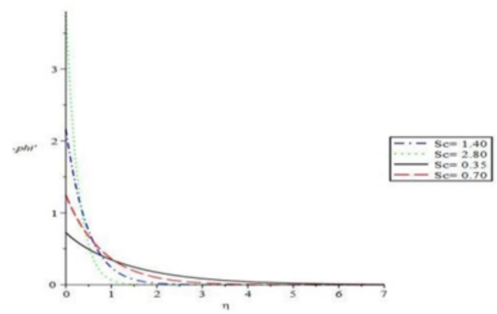

Fig 22 Schmidlt number, Sc on ϕ’

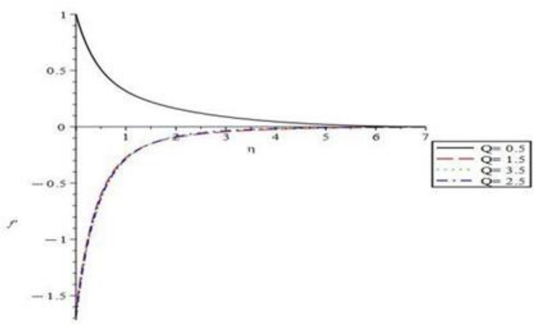

Fig 19 thermal heat generation, Q on f’

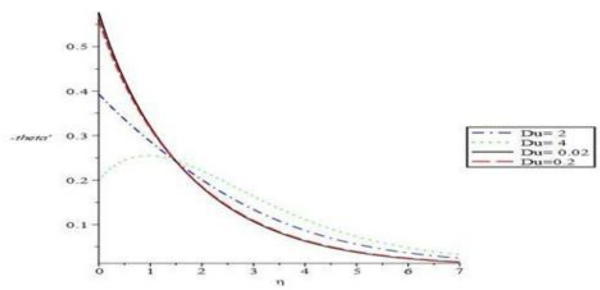

Fig 23 Dufour, Du on θ

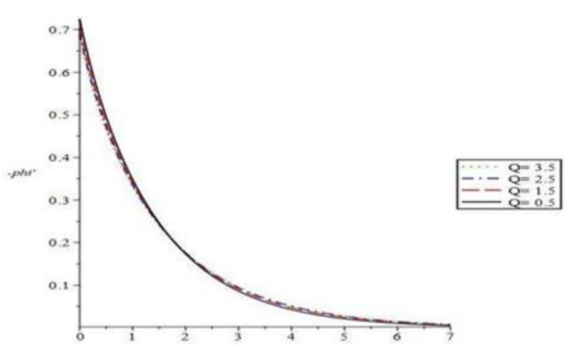

Fig 20 thermal heat generation, Q on ϕ’

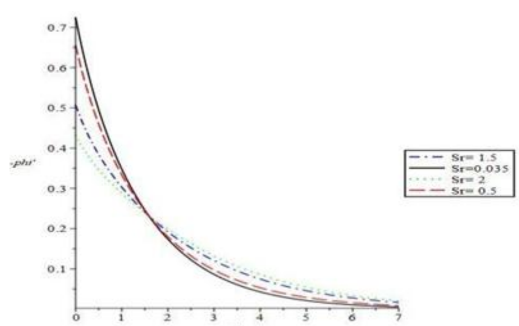

Fig 24 soret, Sr on ϕ’

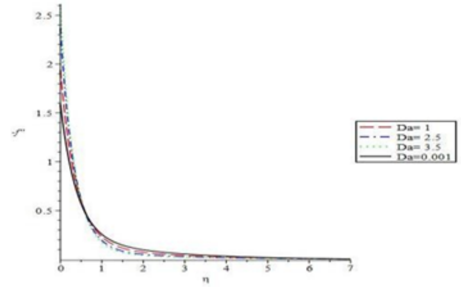

Fig 25 Darcy number, Da on f’’

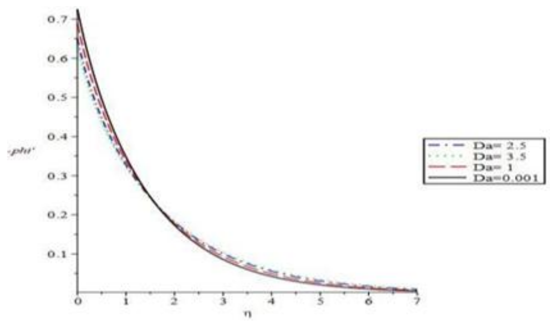

Fig 26 Darcy number, Da on ф’

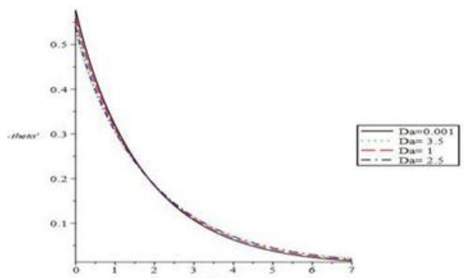

Fig 27 Darcy number, Da on θ

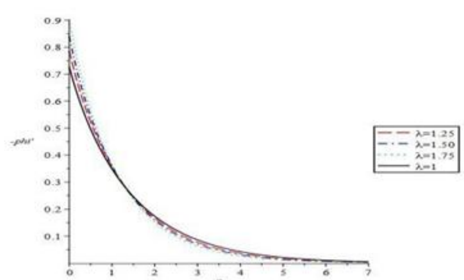

Fig 28 rate of viscoelasticity, λ on ф’

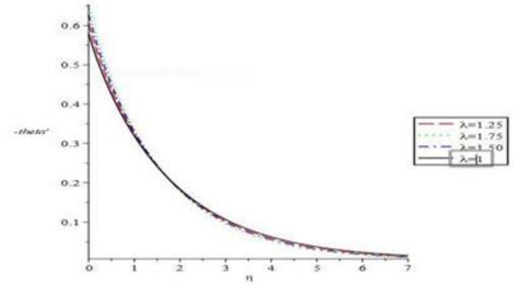

Fig 29 rate of viscoelasticity, λ on θ

II. DISCUSSION

Figures 1, shows the magnetic field effects on fluid flow on the velocity profile, showing that an increase in the value of M leads to an increase in the velocity distribution of the generated energy. Figure 2, also shows that an increase in M lead to an increase in the Nusselt number, that is the ratio of convective to conductive heat transfer at the surface increases. Figure 3, represent the effects of increased value of M on the Sherwood number, that is the ratio of convective to mass diffusive transfer at the surface, which decreases with an increase in M. implying that, temperature and concentration at the boundary layer get thinner as magnetic field increased. Figures 4, present that, an increase in Grashof parameter (Gr) decreases the velocity profile while Figure 5, shows that increase in the ratio of convective to conductive heat transfer at the surface with increase Gr and Figure 6, also shows an increase ratio of convective to mass

diffusive transfer with increase in Gr. This result suggest that slow rate of heat and free convective mass transfer was noticed. In this case, Gr slowed down the temperature and concentration. In Figures 7 to 9, the analysis of Pr are presented. Figure 7 presented that increase in Pr led to increase in velocity profile. Confirming that dimensionless velocity or exponential velocity increased near the surface. Figure 8 similar occurance but with a decrease in Nusselt number. The results shown in Figures 7 and 8 showed that Pr increased the thickness of thermal boundary layer as such heat was unable to move out of the system, hence temperature profile increased. Figure 9 establish that increased in Pr. That is diffusive increased concentration. In Figures 10 to 12, Gc effects on the velocity-profile, energy and concentration respectively. The solutal Grashof effects on velocity distribution was shown in Figure 10. It proved that increase in Gc led to decrease in velocity. The values of energy and concentration increased with variation in solutal Grashof number. These analyses are true of the Figures 10, 11 and 12 due to the fact that Gc usually increase when one talks about free or natural convection thereby increasing boundary layer flow velocity. Figure, 13 and 15 varied effects of Fw on the velocity, energy and concentration profiles respectively. It was found that increase in Fw led to proportional decrease in rate of fluid flow, energy or heat transfer as well as diffusive profile or mass transfer. This parameter has more influence on velocity profile because it explains the concept of porosity or permeability. The negative values explain the concept of suction while positive values of the parameter explain the concept of injection. It was observed that suction decreased the profile velocity, thereby indicating that suction stabilized the boundary layer development. Injection increases the velocity-profile at the boundary layer indicating that injection supports the flow to penetrate more into fluid. In Figure 14, it was found that energy decreased as injection decreased, this suggests that injection does not induce cooling hence, fluid transfers to the surface. On the other hand, energy decreases as suction increases, this implies that suction leads to faster cooling of the plates. Figure 15 presents the fact that diffusion decreases as the suction increases and increases as the injection increases due to respective thinner and thickness in mass boundary layer. Figures 16 to 18 indicate the effects of radiation on the velocity profile, energy and concentration, respectively. It was discovered that increase in radiation parameter, manifest decrease in velocity and concentration profiles. It was obvious that velocity and concentration profiles decreased with increase in radiation parameter, but increase in energy profile. These effects were as a result of thickness in velocity and species boundary layers. The increase in thermal energy was as are result of thickness in thermal boundary layer. Figures 19, 20

and 21, is the varied values of Q, represents the behavior of velocity profile, Nusselt and Sherwood number. In Figure 19 shows an increase in Q parameter increases fluid flow velocity. In Figure 20 it could be seen that increase in Q led to corresponding change in the boundary layer flow. The effect was as a result of heat source in the boundary layer on energy distribution. It was found that variation of Q generates energy which caused the energy of flow to increase/decrease. The presence of heat source in boundary absorbs energy which influenced the Nusselt number of the fluid to increase/decrease, and as it was noticed from the figure the temperature decreased with increase in heat source/sink where $Q > 0$, while it decreased with heat sink $Q < 0$. This case, heat source/sink were experienced. In Figure 21, it was seen that increase in Q led to corresponding increase in sherwood. Figure 22 explained the effects of Sc on concentration, which shows that an increase in Sc led to decrease in concentration profile. Sc quantifies the relative effectiveness of momentum and mass transport by diffusion in the hydrodynamic or velocity and concentration boundary layers. Figure 23 explains the effects of dufour on energy, and showed increase in exponential temperature, led to increase in the Nusselt number. Figures 24 explained the effects of varied Soret parameter on the exponential concentration profiles. It was found that increase in Sr. led to decrease in velocity, energy but an increase in the specie or concentration distribution. This means that Sr. cannot be neglected in explaining fluid flow, heat and mass transport phenomena. The present results compared favorably with existing literatures; similarities/contrasts were noticed with minimal errors. The reasons for the minimal errors might be due to the method or technique used in solving the problems as well as the parameters we added to the new models solved. Figure 25 to 27 present the effects of exponential velocity, temperature and specie when Darcy porosity was varied. It was discovered that increase in Da led to increase in fluid velocity but decrease in temperature and concentration profiles. There were distinct changes observed in momentum and thermal boundary layers while minute changes occurred in concentration boundary layer when Darcy porosity parameters were varied. This result probably follow the convectional flow where both shear layer, thermal and boundary layer have similar characteristics but in cases where heat transfer is influenced by conduction or radiation. The boundary layer for the velocity, temperature profile and concentration exhibited varied behavior. Figures 28 to 29 displayed the behavior of λ and its effects on temperature and concentration, respectively. As the λ parameter varies increasingly, the skin friction coefficient and Nusselt increased but decreased Sherwood numbers. The clear implication of the plots showed decrease in velocity, temperature and concentration profiles.

CONCLUSION

The parametric effects on heat and mass transfer of steady MHD viscoelastic fluid flow with cross-diffusion in porous media involving free convective fluid, heat and mass transfer, with thermal radiation in analyzing the nonlinear steady MHD viscoelastic fluid flow in the porous media using the similarity transformation to arrive at a set of ODEs were obtained from the governing equations. The momentum equation and equation of concentration were solved numerically using Maple 2024. The study concluded that solutal Grashof, thermal Grashof, magnetic parameter, radiation parameter, Dufour and Soret numbers had significant effects on steady MHD viscoelastic fluid flow in porous media.

REFERENCES

[1] Amoo, S. A. (2022), Modelling Thermo-physical Effects of Heat and Mass Transfer in Unsteady MHD Viscoelastic Fluid Flow in inclined Porous Media. N igerian Journal of M athematics and Applications, 32, 103 − 116.

[2] Amoo, S.A. and Idowu, A.S. (2018). Cross Diffusion effects on heat and mass transfer of magnetohydrodynamics flow in porous media over exponentially stretching surfaces. In FUW trends in science and Technology, 3 (2A), 450-460.

[3] Gizachew, A. and Shankar, B. (2018), MHD Flow of Non-Newtonian Viscoelastic Fluid on Stretching Sheet With The Effect of Slip Velocity. International Journal of Engineering and Manufacturing Science. ISSN 2249-3115 (8)1 1-14

[4] Hayat, T. and Sajid, M. (2008). Analytic solution for axi-symmetric flow and heattransfer of a second grade fluid past a stretching sheet. Int. J. Heat Mass Transfer, 50, 75-84.

[5] Heydari, M. R. and Taleghani, A. S. (2016), Analysis of boundary layer in MHD flow of non- Newtonian visco-elastic fluid on stretching sheet, Bulletin de la Société Royale des Sciences de Liège, 85, 21 - 33.

[6] Ibrahim S. Y. and Makinde O. D. (2010). Chemically reacting MHD boundary layer flow of heat and mass transfer over a moving plate with suction. Scientific Research and Essays, 5(9), 2875-2882.

[7] Ibrahim, S. M. and Suneetha, K. (2015). Effect of heat generation and thermal radiation on MHD flow near a stagnation point on a linear stretching sheet in porous medium and presence of variable thermal conductivity and mass transfer. Journal of Comp. and Appl. Res. Mech. Engr. 4(2): 133-144.

[8] Kala, B. S., Singh, M. and Kumar, A. (2014). Steady MHD free convective flow and heat transfer over nonlinearly stretching sheet embedded in an extended Darcy Forcheimmer porous medium with viscous dissipation. J. Global Res. Math. Achives, 1-5.

[9] Mfebe, J. F., Amoo, S. A. and Anyanwu, E. O. (2025), Analysis of cross-diffusion effects on heat and mass transfer of unsteady magnetohydrodynamics viscoelastic fluid flow in exponentially- stretching vertical and inclined porous surfaces. A dissertation report in the department of mathematics, FUW, wukari, Nigeria.

[10] Nandeppanavar, M. M., Vajravelu, K. and Abel, M. S. (2011), Heat transfer in MHD viscoelastic boundary layer flow over a stretching sheet with thermal radiation and non-uniform heat source/sink, Communications in Nonlinear Science and Numerical Simulation, 16, 3578-3590.

[11] Sidheswar, P. G. and Mahabaleswar, U. S. (2005), Effect of radiation and heat source on MHD flow of a visco-elastic liquid and heat transfer over a stretching sheet, Int. J. Non-Linear Mech. 49, 807–820.